Polymer Degradation and Stability 181 (2020) 109292

Contents lists available at ScienceDirect

Polymer Degradation and Stability

journal homepage: www.elsevier.com/locate/polydegstab

Synergistic effect between histidine phosphate complex and hazelnut shell for flammability reduction of low-smoke emission epoxy resin

K. Salasinska [a, *], M. Celiński [a], K. Mizera [a, b], P. Kozikowski [a], M.K. Leszczyński [c], A. Gajek [a]

[a] Central Institute for Labour Protection – National Research Institute, Department of Chemical, Biological and Aerosol Hazards, Warsaw, Mazovia, Poland
[b] Warsaw University of Technology, Faculty of Materials Science and Engineering, Warsaw, Mazovia, Poland
[c] Polish Academy of Sciences, Institute of Physical Chemistry, Kasprzaka 44/52, 01-224, Warsaw, Mazovia, Poland

ARTICLE INFO

Article history:
Received 17 March 2020
Received in revised form
17 June 2020
Accepted 29 June 2020
Available online 22 July 2020

Keywords:
Fire behaviour
Fire retardant
thermal Stability

ABSTRACT

A novel intumescent fire retardant (FR) system based on ground hazelnut shell (HS) and L-histidinium dihydrogen phosphate-phosphoric acid (LHP) was introduced into the epoxy resin (EP) in order to verify their effectiveness as fire retardant. The burning behaviour and smoke emission were assessed with cone calorimeter (CC) and UL-94 tests. Furthermore, the analysis of volatile products evolved during both the thermal decomposition and burning was conducted with the use of thermogravimetric analysis (TGA/FT-IR) and steady-state tube furnace (Purser/FT-IR), both combined with FT-IR with the use of a transfer line. It was found that the system containing 5 wt% of HS and 15 wt% of LHP lead to in the formation of a swollen char with numerous closed cells, which reduced the burning process as well as smoke emission. The obtained results confirm the occurrence of a synergistic effect between the components.

1. Introduction

The production of epoxy resins (EP) accounts for about 70% of the thermosetting polymer world's market (excluding polyurethanes). The value is so high mostly due to the wide application of EP in the production of composites, electronic insulation elements, coatings and adhesives [1–3]. This is the result of a combination of good mechanical and electrical properties, good adhesion, low shrinkage during curing, resistance to high temperatures and chemicals [4,5]. On the other hand, EP is characterized by high flammability, hence the research for new solutions in the field of fire retardants dedicated to EP.

Intumescent fire retardants (IFRs) are considered to be one of the most effective FRs for polymers. When a material containing IFR burns, a swollen carbonaceous layer acting as a physical barrier for the transfer of heat and matter between the gas and the condensed phase is formed. The advantages of using IFRs also include the reduction of smoke emission and toxicity of the emitted decomposition and combustion products as well as the absence of burning droplets [6]. Jian et al. [7] have developed a system of a novel organophosphorus heteroaromatic compound (DMBT), which was synthesized from 2-mercaptobenzothiazole (MBT) and 9,10-dihydro-9-oxa-10-phosphaphenanthrene-10-oxide (DOPO), and designed for epoxy resins. Good char forming ability translated into V-0 rating in UL-94 test, low the LOI value of 33.5%, as well as an effective reduction in the heat release rates (HRR) and total heat release (THR) during CC tests. Mu et al. [8] have developed phosphorus-containing flame retardant wrapped covalent organic frameworks (FCOFs) nanosheets. The LOI and UL-94 vertical burning rating of EP with 3.2 wt% of FCOFs was 25.5% and V1, respectively. The peak of heat release rate (pHRR) stated for EP with 3.2 wt% of FCOFs decreased by ~ 20% in comparison with the neat sample. Moreover, Markwart et al. [9] have developed aromatic and aliphatic, hyperbranched, halogen-free polyphosphoesters (hbPPEs) which were synthesized by olefin metathesis polymerization and investigated as a FR in epoxy resins. The aliphatic FRs were found to be more effective for EP than the aromatic ones due to their greater overlap in the decomposition temperature and thus better matrix interaction. This resulted in a stronger reduction of pHRR and FIGRA in comparison to the resins with aromatic FRs.

Modern halogen-free fire retardants are mainly based on organic aromatic structures with a high content of nitrogen- or phosphorus-based substituents. Most of these compounds are being obtained through multistage reactions, creating large amounts of substances that are harmful to the environment. Therefore, given the ecological aspect, there is an unquestionable need to find

* Corresponding author.
E-mail address: kamila.salasinska@ciop.pl (K. Salasinska).

https://doi.org/10.1016/j.polymdegradstab.2020.109292
0141-3910/

Abbreviation

10HS/10LHP	epoxy resin with 10 wt% of HS and 10 wt% of LHP
15HS/5LHP	epoxy resin with 15 wt% of HS and 5 wt% of LHP
5HS/15LHP	epoxy resin with 5 wt% of HS and 15 wt% of LHP
20APP	epoxy resin with 20 wt% of APP
20HS	epoxy resin with 20 wt% of HS
20LHP	epoxy resin with 20 wt% of LHP
APP	ammonium polyphosphate
Ar	aspect ratio
CC	cone calorimeter
D	equivalent diameter
DMTA	dynamic mechanical thermal analysis
EHC	effective heat of combustion
E_n'	storage modulus
EP	epoxy resin
FR	fire retardant
HB	horizontal burning
H NMR	proton nuclear magnetic resonance
HRR	heat release rate
HS	hazelnut shell
IFR	intumescent flame retardant
LHP	L-histidinium dihydrogen phosphate-phosphoric acid
LOI	limited oxygen index
MAHRE	maximum average rate of heat emission
pHRR	maximum value of heat release rate
PXRD	powder X-ray diffraction
SEA	specific extinction area
SEM	scanning electron microscope
$T_{5\%}$	temperature of 5% mass loss
tan δ	loss factor
Tg	transition temperature
TGA	thermogravimetric analysis
TGA/FT-IR	thermogravimetric analysis connected with Fourier-transform infrared spectroscopy
THR	total heat release
T_{maxn}	temperature of the maximum degradation rate
TSR	total smoke release
TTI	time to ignition
U_{800}	residue at 800 °C
UL-94	underwriter laboratories

alternative, eco-friendly products whose production and use would not pose a threat to the natural environment. The use of natural materials as components in FR systems for polymers is an innovative idea [10]. In our earlier work [11] we found that ground hazelnut and walnut shell, as well as sunflower husk, can be used as a cheap fillers for EP and increase the ecological value of the product, as well as reduce its flammability and smoke emission. An introduction of properly prepared hazelnut shell into the resin and exposing the material to the heat flux causes the formation of a carbonaceous layer with a cellular structure, characteristic for IFRs. In order to enhance the FR's properties of the plant filler, the HS was mixed with the developed intumescent FR, namely L-histidinium dihydrogen phosphate-phosphoric acid (Patent Application P.426677 [12]).

This paper provides an analysis of the thermal and fire properties of an EP modified with a novel FR system consisting of HS and the developed IFR. The burning behaviour of gained materials, varying in amount of IFR system, were compared to the unmodified EP and EP with commercial IFR. This approach is particularly promising, considering the world production of hazelnut, which in 2018 have reached the value of 863,888 tonnes, including 173,946 tonnes in Europe (6642 tonnes in Poland).

2. Experimental

2.1. Materials

Compounds used in the synthesis of L-histidinium dihydrogen phosphate-phosphoric acid were purchased from Apollo Scientific (histidine >99%) and Honeywell (85% conc. phosphoric acid). The substrates used for the polymer matrix were as follows: epoxy resin Epidian 624 (epoxy number 0.48–0.51 mol/100 g, viscosity 600–800 mPa s) and curing agent IDA (amine number 250–350 mgKOH/g, viscosity 150–300 mPa s) purchased from Ciech Sarzyna S.A. Hazelnut shell (Corylus avellana species, HS) was purchased from AGRO Jarosław Seroczynski. The chemical composition of ground hazelnut shell was as follows: cellulose approx. 38%, hemicellulose approx. 20%, lignin approx.39%, fat approx. 2%, protein approx. > 0.2% [13]. Furthermore, ammonium polyphosphate (APP) was used to manufacture a reference material IFR.

Synthesis of L-histidinium dihydrogen phosphate-phosphoric acid (LHP). Initially 78 g (0.5 mol) of L-histidine and 100 ml H_2O was placed in a 1000 ml beaker, equipped with a mechanical stirrer. The mixture was heated to about 50 °C in order to dissolve the amino acid. Next 115 g (1 mol) of 85% phosphoric acid solution (V) was introduced into the mixture (Fig. 1), heated up to 80 °C and stirred for 4 h. Then the heating was switched off and the mixture was left to cool down while constantly stirred. After 2 h the crystallization process was observed. Then 30 min later approx. 400 ml of cooled methanol was added to the mixture. After 15 min the precipitate was filtered. The precipitate was washed twice with 50 ml of cooled methanol and left to dry. The amount of the obtained product was about 167 g (95% yield). The structure was confirmed by NMR: δ in D_2O [ppm]: 8.65 (s, 1H, N-C*H*-), 7.38 (s, 1H, N-C*H*-), 4.06 (t, 1H, CH_2-C*H*-), 3.34 (d, 2H CH_2-CH-) (Fig. 2), as well as PXRD analyses described in a separate article [14], using literature reference data [15].

Preparation of the natural filler. The grinding of the hazelnut shell was conducted on a laboratory sieve mill MUKF-10 from Młynpol P.P.H. using a sieve with a size mesh of 0.2 mm, while the drying process was performed with the use of a Plus II Incubator for at least 3 days in 70 ± 2 °C.

Preparation of the materials. Epidian 624 and LHP were mixed thoroughly using a high speed mechanical stirrer proLAB 075 from GlobimiX Ltd., equipped with a water jacket and vacuum venting system. The stirring was performed with the use of the following rotational speeds: 3000, 5,000, 8,000 and 10,000 rpm applied for approx. 5, 4, 3, and 3 min, respectively. Next, the HS was introduced and the composition was mixed again in the same conditions. Afterwards, IDA was added and stirred at 3,000 and 5,000 for 1 and 0.5 min. Then, the mixture was poured into moulds, the samples were cured at ambient temperature for about 24 h as well as post-cured at 70 °C for 3 h and conditioned at room temperature for 2 weeks. Other samples were prepared according to the procedure described above depending on the presence of the natural and/or synthetic component. The samples from the unmodified epoxy resin (EP) as well as with 20 wt% of ammonium polyphosphate (APP), as reference materials, were also prepared. The compositions of each material from the series are presented in Table 1.

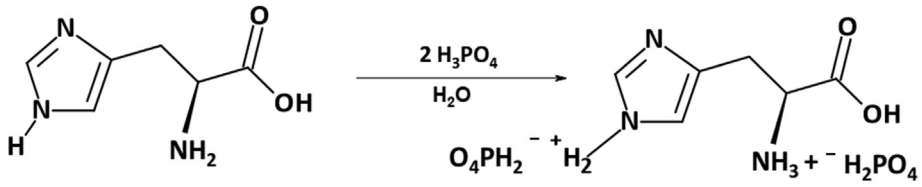

Fig. 1. Synthesis course for L-histidinium dihydrogen phosphate-phosphoric acid (LHP).

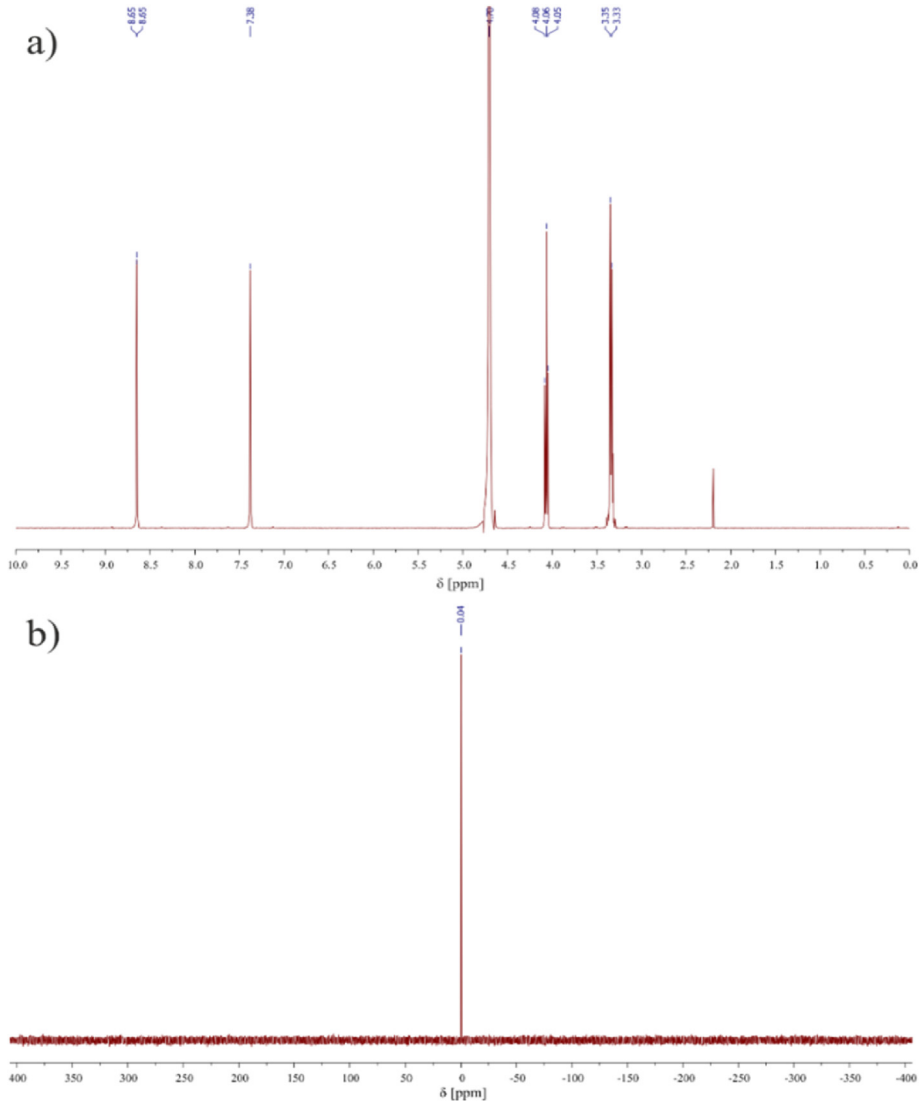

Fig. 2. a) ^{1}H NMR of LHP in D_2O, b) ^{31}P NMR of LHP in D_2O. Note: only one signal in the ^{31}P NMR spectrum indicates fast proton exchange between $H_2PO_4^-$ and H_3PO_4.

Table 1
Designations and compositions of manufactured materials.

Sample	Filler type	Filler content, wt%
EP	–	–
20APP	APP	20
20LHP	LHP	20
20HS	HS	20
15HS/5LHP	HS, LHP	15/5
10HS/10LHP	HS, LHP	10/10
5HS/15LHP	HS, LHP	5/15

2.2. Methods

^{1}H and ^{31}P NMR spectra were recorded at room temperature using a Varian Mercury 400 MHz NMR spectrometer using *ca* 10 mg of the analysed material, which was dissolved in 0.6 ml of D_2O prior to analysis.

Investigations of HS and LHP particles as well as materials fracture surface were conducted using an SU8010 scanning electron microscope from Hitachi. The sample was coated with gold using a Quorum Technologies Q150T ES sputterer. A quantitative analysis of the particles of the components was conducted using ImageJ program allowing to obtain an equivalent diameter (D) and aspect ratio

(Ar). Following cone calorimetry the samples were also investigated, but did not require sputter coating. To investigate the chemical composition of the residue point an elemental analysis was conducted using the Thermo Scientific NORAN System 7 from Thermo Scientific UltraDry, equipped with an electrically cooled Silicon Drift Detector EDS detector. All observations were conducted at an accelerating voltage of 10 kV.

The DMTA tests were performed using Q800 equipment from TA Instruments. Investigations were conducted with a 3 point bending method with a constant frequency of 1 Hz and a strain of 0.01%. All samples were evaluated in the temperature range from 20 to 160 °C with the heating rate of 2 °C/min.

The thermal decomposition was studied in nitrogen using the thermal analyser TGA Q500 from TA Instruments Ltd. The 10 mg samples were heated at the rate of 10 °C/min from room temperature to 800 °C. The flow rate of gas was 10 ml/min in the chamber and 90 ml/min in the furnace.

Flammability was examined by fire hazard test performed in accordance to IEC 60695-11-10 standard (test method A – horizontal burning). Three horizontally supported samples from each series (125 × 10 × 4 mm) were subjected to a 50 W test flame.

The fire behaviour was assessed using a cone calorimeter from Fire Testing Technology Ltd. in accordance with ISO 5660-1. The samples (100 × 100 × 6 mm) were irradiated horizontally at a heat flux of 35 kW/m^2. The separation space between samples and the heater was set to 25 mm. After tests, the residues were photographed using a digital camera EOS 400 D from Canon Inc.

The TGA was coupled with a Fourier transform infrared spectroscopy Nicolet 6700 spectrometer from Thermo Scientific (TGA/FT-IR) to study the formation of volatiles produced in the thermal decomposition process. Samples of about 10 mg were heated in air from room temperature to 860 °C at a rate of 20 °C/min. The FT-IR gas cell was held at 240 °C and the temperature of the transfer line was set to 250 °C. The analyses were performed in the spectral range of 400–4000 cm^{-1} and resolution of 4 cm^{-1}.

To study the formation of the produced volatiles a state tube furnace method (Purser Furnace), simulating fire conditions was used, in conformity with ISO/TS 19700:2007. Samples (10 g) of the tested materials were placed in a quartz mould and put into the pre-heated furnace at 25 °C. Then the samples were heated to 860 °C with air flow 20 L/min. The tube was coupled with the FT-IR from Bruker Tensor 27 FTIR.

3. Results and discussion

3.1. Size determination

Fig. 3 shows SEM images of particles of LHP and HS before introducing them to the EP.

SEM images allow to observe that particles of the components of the developed FR system were varied in terms of size and geometry. Single particles of L-histidinium dihydrogen phosphate-phosphoric acid resembled plates, however, Fig. 3 shows mainly agglomerates, resulting from their grafting. In the case of HS, particles with a slightly elongated shape and a fairly smooth surface were dominant (Fig. 3b).

The equivalent diameters (D) distributions of the particles of the FR system components, calculated from SEM images, are shown in Fig. 4. HS particles exhibit narrower D distributions with the average value 20.9 μm, while the synthetic component of the FR system is over twice a size of HS (46.2 μm). Additionally, the aspect ratio (Ar) for both components was determined (Fig. 5). It was found that the average value of Ar reached 1.71 and 1.57 in the case of ground hazelnut shell and L-histidinium dihydrogen phosphate-phosphoric acid (Table 2), respectively. This suggests that LHP particles are slightly more circular compared to HS. The higher average D value as well as its wider distribution are associated with LHP's tendency to agglomerate and may hinder the interaction between the FR components.

3.2. Microstructure analysis

Microstructure observations of the unmodified resin and EP/IFRs were conducted using SEM. Images of the fracture surface of the investigated materials, taken at a magnification of 500x, are shown in Fig. 6.

The SEM analysis revealed the presence of particles of the fire retardant system in the whole volume of materials and their uneven distribution. It was observed that the size of the natural component's particles coincides with the size of the particles before introducing them to the polymer (Fig. 3), which was not the case with L-histidinium dihydrogen phosphate-phosphoric acid. This is due to the mixing process conducted using high speed mechanical stirrer, that contributed to the destruction of the agglomerates of LHP. Such effect was not observed at lower rotational speeds of the stirrer [10,14], thus there was no synergistic effect between the components of the FR system. The low molecular weight of the epoxy resin contributed to the increase in the wettability of the surface of the FR system components, therefore only a few voids located near the surface of the tested samples were observed. The voids visible in the interphase are related to the destructive forces that occurred during the preparation of the test samples. These voids, as well resulting from particles' loss, as in the case of 20APP (Fig. 6b), suggest limited adhesion between FR particles and epoxy resin.

3.3. Mechanical properties

Mechanical properties were tested by dynamic mechanical thermal analysis, while storage modulus (E') as well as loss factor

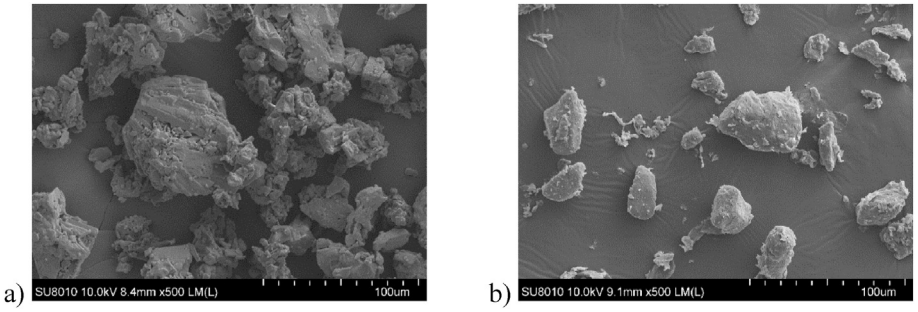

Fig. 3. Particles of the components of developed fire retardant system: L-histidinium dihydrogen phosphate-phosphoric acid (a) and hazelnut shell (b), mag. 500x

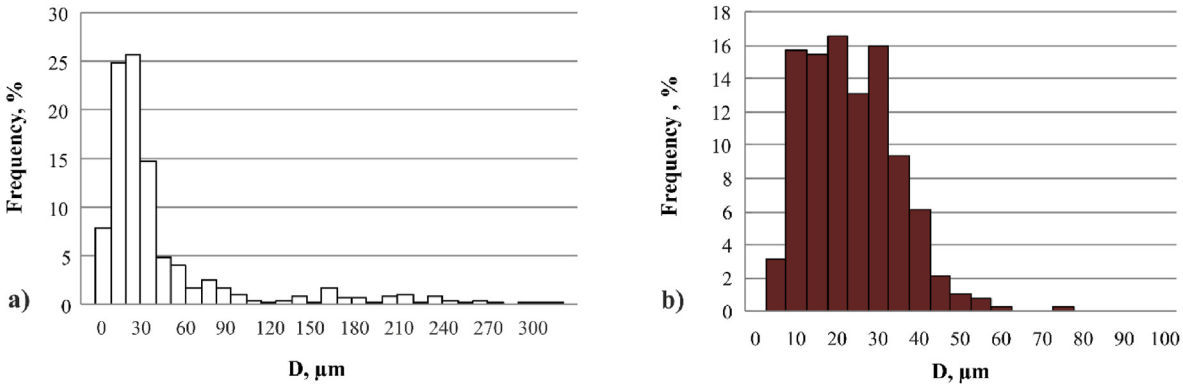

Fig. 4. D distribution of particles of LHP (a) and HS (b).

(tan δ) curves are presented in Fig. 7.

The addition of all substances caused an increase in E′ in the considered temperature range, and the highest values were obtained for materials containing at least 15 wt% ground hazelnut shell (Table 3). Samples with IFRs reveal a higher ability to maintain mechanical loading with recoverable viscoelastic deformation than EP, also in elevated temperatures, which may be assigned to improved stiffness [16]. However, a decrease in E′ with a growing amount of LHP in the developed system, being the result of lower rigidity of synthetic compound compared to HS particles, was also observed. An increase in E′ in materials with HS is connected with the structure of shell, as well as the chemical constitution of the filler, especially a high amount of lignin, which is responsible for lingo-cellulosic material stiffness [11,13]. Moreover, the addition of IFRs caused a small decrease in the transition temperature (Tg). 20LHP was the only exception for which Tg temperature slightly increased. This effect may be assigned to better adhesion in the interfacial region between LHP and EP [17]. The decrease of the Tg in materials with HS is connected with residual fat in the filler, which plasticized the materials [18]. This change was not accompanied by an E′ decrease. Therefore, it may be stated that used filler did not modify the curing process in the entire polymer material; it only led to a modification of the cross-link density near the organic particles' surface [18]. The crosslink density of resin and EP with IFRs can be obtained by the classical theory of rubber elasticity model [19] under the glass transition temperature (Tg) by the following equation:

$$\upsilon_e = \frac{E'}{3\varphi RT}$$

where E′ is the storage modulus at Tg+50 K, and φ usually can be seen as 1, and the value R is 8.314 J mol^{-1} K^{-1} (Table 3). The crosslink density of the EP increased for all materials with IFRs. The highest values were recorded for samples containing a significant amount of HS. High crosslink density usually contributes to promoting high strength and modulus [20], resulting in improved strength and high modulus in the case of 20HS and 15HS/5LHP.

Table 2
Equivalent diameter and aspect ratio values of novel IFR system components.

Sample	D, µm	Ar
HS	20.9 (11.2)	1.71 (0.4)
LHP	46.2 (54.5)	1.57 (0.3)

3.4. Thermal stability

The aim of the thermogravimetric analysis was to assess the thermal stability of the epoxy resin with the novel FR system. The results of the TG analysis are presented in Table 4 and Fig. 8. The additional TG and DTG curves of the LHP and HS are presented in Figs. S1–S2 in the Supporting information section.

The highest values of 5% mass loss ($T_{5\%}$), compatible to the onset temperature of decomposition, were determined for EP modified with HS or FR system containing them (with the exception of 10HS/10LHP). Values noted for EP with APP and LHP were lower, however, examples of polymers with synthetic IFRs decaying at lower temperatures, attributing to the formation of char, can be found in the literature [16,18,21].

The most intense decomposition of epoxy resin occurred above 300 °C, which corresponds to the decomposition of the aromatic group of the epoxy resin and the aliphatic amine from the curing

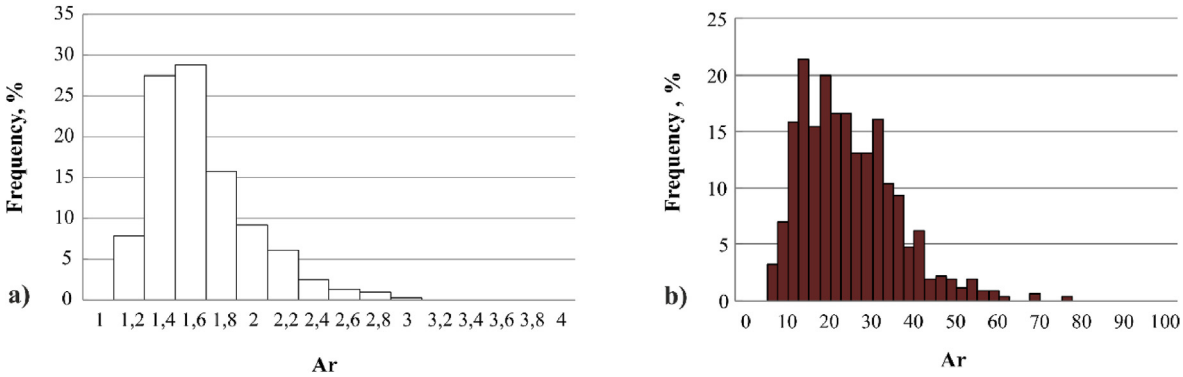

Fig. 5. Ar distribution of particles of LHP (a) and HS (b).

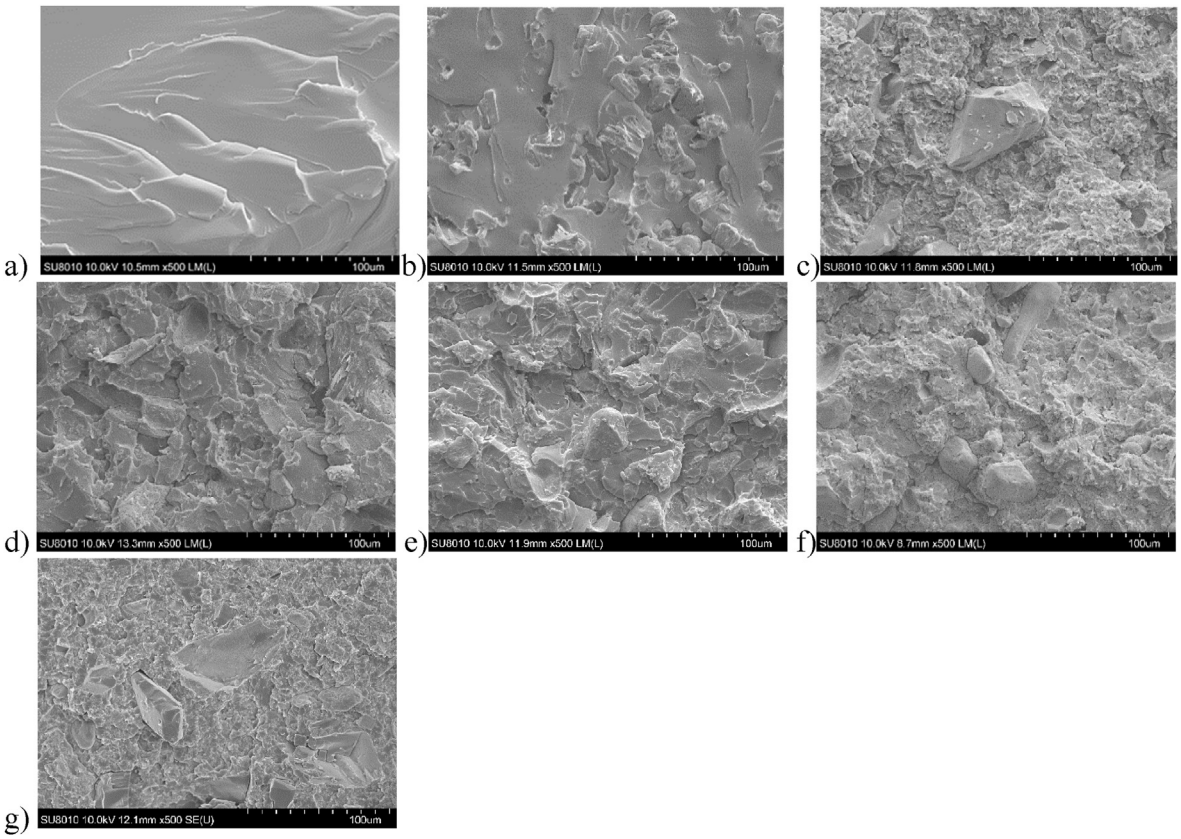

Fig. 6. SEM images of breakthroughs of EP (a), 20APP (b), 20LHP (c), 20HS (d), 15HS/5LHP (e), 10HS/10LHP (f), 5HS/15LHP (g), mag. 500x

agent (T_{max3} and T_{max4}) [22]. In the case of the investigated materials, except for HS, the stages of decomposition shifted towards lower temperatures. However, the rates of decomposition are lower than for the unmodified polymer. The additional steps corresponding to the dehydration of phosphoric acid [23] and decomposition of hemicellulose (T_{max2}) in the case of LHP and HS [11], can be observed (Figs. S1–S2). The decay of the other components, such as histidine from LHP or lignin and cellulose from HS, overlaps with the decomposition of EP causing a shift of T_{max} values mainly towards lower temperatures. In turn, the stages of decomposition above 400 °C correspond to the decomposition of transient char (T_{max5}-T_{max7}) [24]. The residual mass (U_{800}) in the case of EP modified with novel fire retardant system was several times higher compared to the neat epoxy resin, and the highest values of U_{800} were determined for 20LHP and 5HS/15LHP. On the other hand, the lower value of this parameter in the case of APP is associated with the decomposition of char, unstable in higher temperatures (additional decomposition at approx. 800 °C). EP with the developed FR system was characterized by a greater thermal stability at higher temperatures, thus resulting in a higher yield of char. The improvement of the charring ability is beneficial to the fire retardancy of epoxy resin [7]. The resin modified with 5 wt% of HS and 15 wt% of LHP showed the highest thermal stability among the tested materials. The synergy between components caused an increase in the onset temperature value, and a decrease in the rate of decomposition in each stage, as well as a simultaneous growth in the yield of char.

3.5. Flame retardancy

3.5.1. Reaction to small flame

The flame retardancy was determined by the fire hazard testing, using the horizontal burning (HB) test method, and the results are listed in Table 5 and Figs. S3–S4. As can be seen, all samples were included in the HB class, however, only the unmodified EP and resin with HS demonstrated the ability to burn after the flame was removed. EP burnt intensively, and the process was accompanied by the release of significant amounts of black smoke and dripping (Fig. S3). The introduction of HS reduced the burning intensity as well as smoke emission, moreover, the formation of char was observed. In the case of other materials self-extinguishing, before the flame reached the first marker or immediately after removal of the burner, was noted. Self-extinguishing after the removal of the burner, similar to the commercially available APP, was observed only for EP with 10HS/10LHP and 5HS/15LHP. These results suggest that the minimum amount of LHP is 10 wt % (Fig. S4).

3.5.2. Burning behaviour

To determine the burning behaviour, the investigated materials have been examined with the use of a cone calorimeter, which simulates an open, well-ventilated fire scenario [7]. Table 6 presents average values of fire hazard parameters, while Figs. 9 and 12 show corresponding heat release rate (HRR) and total smoke release (TSR) curves over time.

The introduction of all flame retarding additives resulted in a shorter time to ignition (TTI). Intumescent fire retardants consist of three components, including oxyacid (in LHP case it's a phosphoric acid), accelerating the decomposition of the organic compound in lower temperature range. Thanks to this behaviour shorter chains does not evaporate straight to the gas phase, but are allowed to cyclize and form thermally stable aromatic compounds which are a basis for the char. The presence of phosphorus content in LHP and APP induced the decomposition of polymer during burning [25]. Lower TTI was also observed in the case of resin modified with HS.

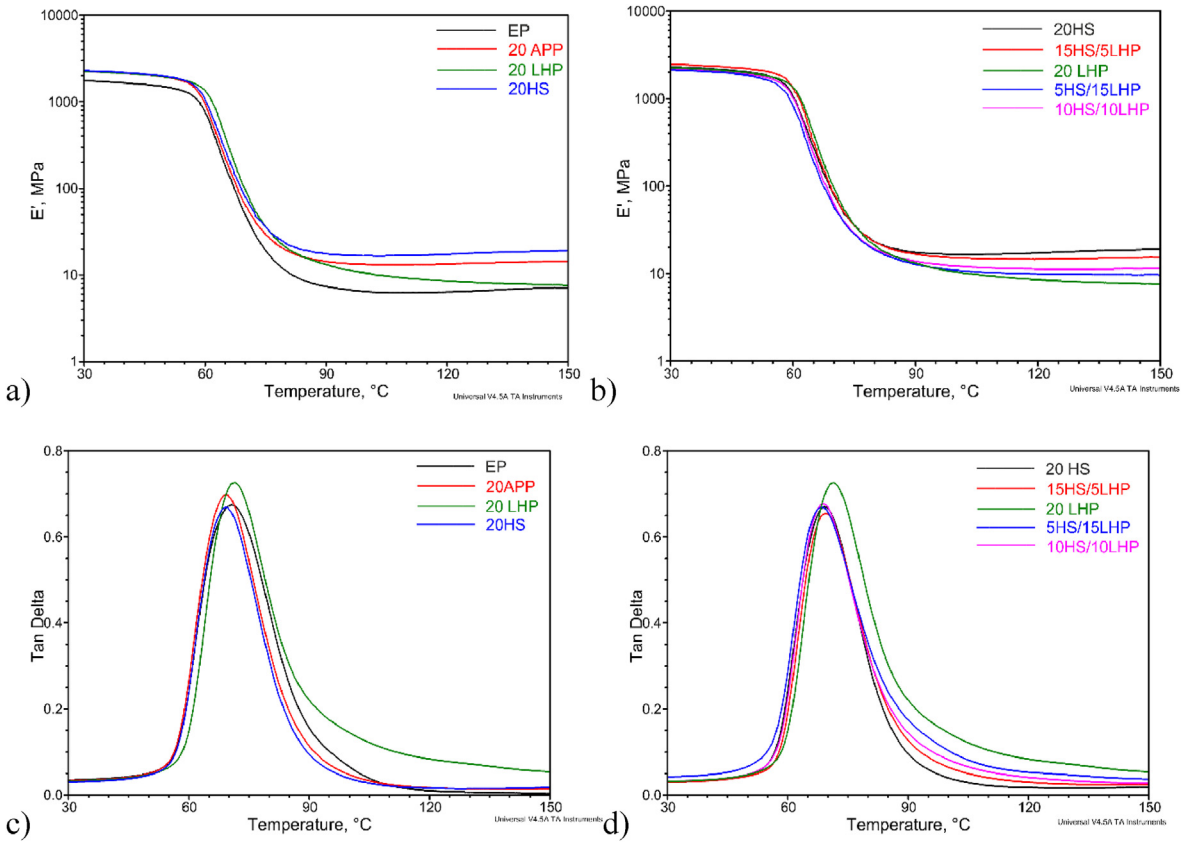

Fig. 7. DMTA curves of E' (a, b) and tan δ (c, d) vs. temperature of unmodified epoxy resin (EP) and epoxy resin with IFRs.

Table 3
Thermomechanical parameters of EP with FR system.

Sample	E'_{30}	E'_{80}	E'_{140}	E'_{Tg+50K}	Tg	tan δ in Tg	υe
	MPa	MPa	MPa	MPa	°C	–	$(mol \cdot m^{-3}) \cdot 10^3$
EP	1767	11	7	6.3	70.6	0.684	0.6
20APP	2257	19	14	13.3	69.2	0.714	1.4
20LHP	2262	21	8	8.4	71.1	0.741	0.9
20HS	2298	23	19	17.2	69.3	0.684	1.8
15HS/5LHP	2474	23	15	14.7	69.3	0.669	1.5
10HS/10LHP	2214	19	11	11.3	68.9	0.693	1.2
5HS/15LHP	2120	19	10	9.9	68.4	0.681	1.0

The maximum HRR (pHRR) values for EP reached 1063 kW/m^2, while for EP with additives they were notably reduced. The most favourable results were obtained for 20LHP and 5HS/15LHP, where the pHRR values (approx. 170 kW/m^2) were over six times lower. The course of the curves was characteristic for samples showing the ability to form a carbonaceous char. PHRR/t(PHRR), defined as the ratio of pHRR to time to achieve it, is regarded as a significant parameter to assess the hazard of fire spread [7]. The highest reduction of PHRR/t(PHRR) was noted for 20LHP as well as 10HS/10LHP and 5HS/15LHP. Similarly, the lowest values of maximum average rate of heat emission (MARHE), corresponding to the peak of the cumulative heat emission divided by time, were recorded for 20LHP and 5HS/15LHP.

The introduction of the investigated IFR system caused the total heat release (THR) to be significantly reduced and eventually dropped from 114 to 35 MJ/m^2 (70% decrease) for 5SH/15LHP. The gradual reduction of effective heat of combustion (EHC) with the increase of the LHP content in IFR system was also observed, which suggests that LHP inhibited free radicals emission to the gaseous phase. The incorporation of decomposition products into the structure of char was confirmed by the growing amount of residue, and the results, consistent with the TGA data, indicate the fire retardant effect of the FR system in condensed phase. The larger yield of residue, amounted to 54%, was created in the case of 5HS/15LHP. The results of pHRR, MARHE, THR and EHC suggest that a reduction of FR of EP corresponds mainly to the presence of LHP, and the best results can be obtained already for its 15 wt% content.

Table 4
The thermal stability of EP with FR system.

Sample	$T_{5\%}$, °C	T_{max1}, °C; %/min	T_{max2}, °C; %/min	T_{max3}, °C; %/min	T_{max4}, °C; %/min	T_{max5}, °C; %/min	T_{max6}, °C; %/min	T_{max7}, °C; %/min	U_{800}, %
EP	172	206; 0.9	–	338; 12	364; 11	–	–	–	3
20APP	166	169; 0.8	–	321; 13	387; 2	414; 1	434; 1	451; 1	9
20LHP	177	169; 0.7	218; 1	315; 8	332; 8	–	430; 2	–	19
20HS	187	–	294; 2	347; 9	360; 9	–	–	–	12
15HS/5LHP	183	175; 0.7	212; 1	328; 9	349; 7	–	–	–	16
10HS/10LHP	162	165; 0.8	211; 1	324; 8	343; 8	–	–	–	17
5HS/15LHP	190	176; 0.7	219; 1	319; 8	333; 8	–	–	445; 1	18

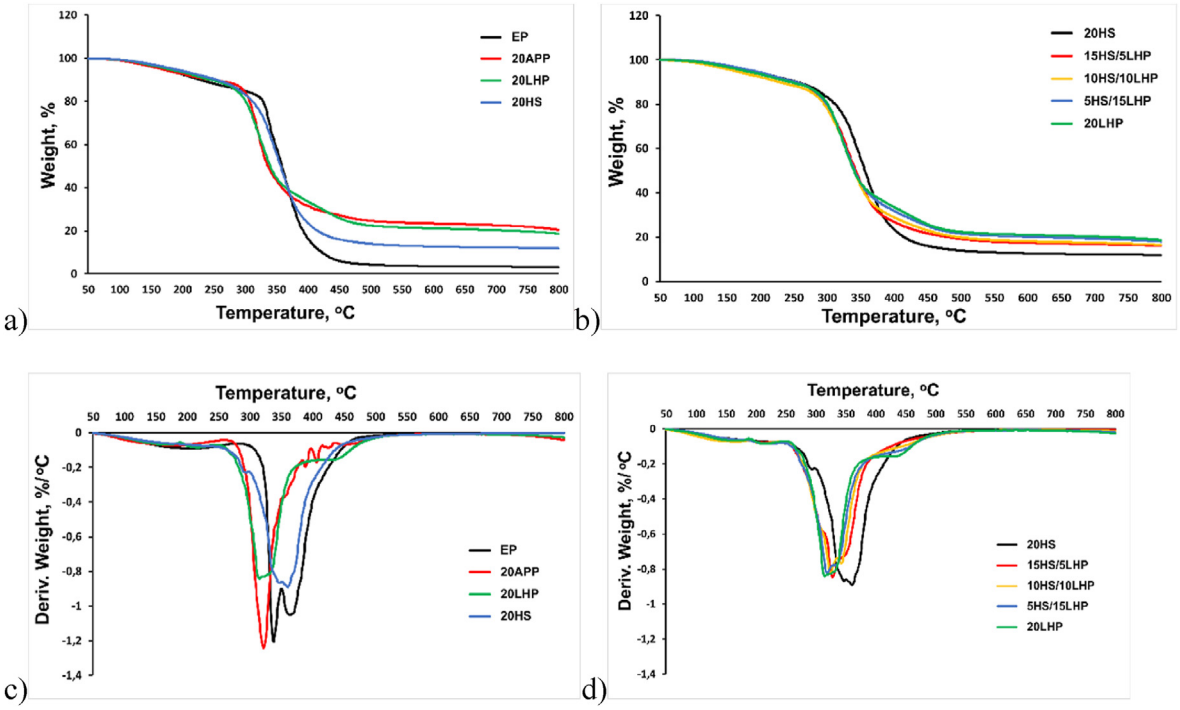

Fig. 8. TG (a, b) and DTG (c, d) curves of EP and EP//IFRs under an inert atmosphere.

Table 5
Horizontal burning test of the EP and the resin with investigated IFRs.

Sample	The linear burning rate, mm/min			Classification
	1	2	3	
EP	17.4	18.7	16.5	HB
20APP	–	–	–	HB
20LHP	–	–	–	HB
20HS	17.6	15.0	15.6	HB
15HS/5LHP	–	–	–	HB
10HS/10LHP	–	–	–	HB
5HS/15LHP	–	–	–	HB

However, the use of hazelnut shell increases the char yield (Table 6) and affects its structure as shown below. In contrast to the resin, which burnt completely (Fig. 10), the remaining materials showed the ability to form a swollen char, preventing the heat and matter transfer between the gaseous and condensed phases. The yield and appearance of the char were strongly determined by the type of the component used, and the largest size (over 10 cm high in the form of a pyramid), characterized by the presence of a tight outer layer, was formed in the case of 5SH/15LHP.

The morphology of the swollen structure was investigated by SEM (Fig. 11). In the case of the EP, only a thin layer with rather smooth outer surface was observed. The use of APP caused a formation of a swollen structure in which open cells and tubules can be observed. While, for 10SH/10LHP and 5SH/15LHP a formation of a highly swollen structure with both open and closed cells similar to the structure of polyurethanes foams [26] was reported (Fig. 11). The presence of hazelnut shell particles exhibiting a swelling ability [11] was necessary to form a highly swollen structure (Fig. S5). Moreover, the obtained data indicated that char comprised mainly C, O, N and P elements. The results suggest that the IFRs were divided into oxides and other decomposition products (section 3.6), resulting in more compact carbonaceous char with better mechanical performance.

One of the most important fire hazard parameters is smoke emission, which is the main cause of death of fire victims (approx. 80%). The lowest specific extinction area (SEA) was recorded for 5HS/15LHP, and the value determined for the material was almost two times lower compared to EP. Similarly, the lowest total smoke release (TSR), equal to 900 m^2/m^2, was noted for 5HS/LHP (Fig. 12), while for the unmodified resin it was as much as 3626 m^2/m^2. The incorporation of decomposition products into the structure of the char as well as their entrapment inside the cells significantly reduced the amount of smoke emitted. The structure formed in the case of 5HS/15LHP was the most effective in preventing the release

Table 6
The cone calorimeter results of EP and EP with investigated substances.

Sample	TTI, s	pHRR, kW/m^2	PHRR/t(PHRR), kW/m^2s	MARHE, kW/m^2	THR, MJ/m^2	EHC, MJ/kg	Residue,%	SEA, m^2/kg	TSR, m^2/m^2
EP	76(2)[a]	1063(83)	5(0)	420(16)	114(1)	26(0)	3(1)	829(26)	3626(125)
20APP	70(6)	262(16)	3(0)	129(8)	53(3)	21(0)	46(5)	643(38)	1627(118)
20LHP	59(4)	166(21)	1(0)	90(8)	37(1)	17(1)	50(4)	459(44)	1016(162)
20HS	63(6)	729(25)	5(0)	402(29)	106(1)	24(0)	3(0)	636(16)	2768(69)
15HS/5LHP	57(72)	577.3(95)	3(0)	305(22)	80(2)	21(0)	13(3)	624(24)	2441(86)
10HS/10LHP	62(8)	282(35)	1(0)	146(9)	51(9)	19(1)	40(9)	461(11)	1238(197)
5HS/15LHP	59(4)	169(13)	1(1)	89(7)	35(4)	17(3)	54(3)	435(30)	899(118)

[a] The values in parentheses refer to standard deviations.

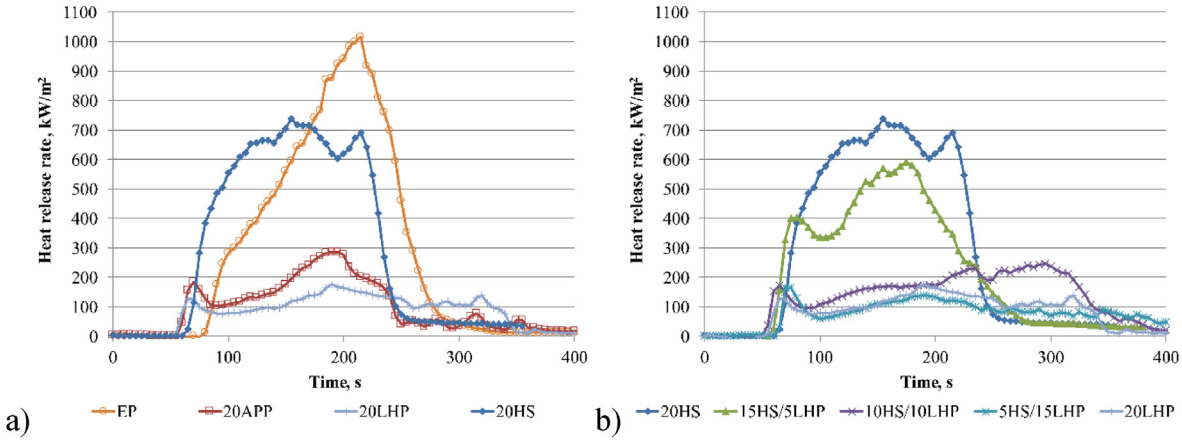

Fig. 9. Representative heat release rate curves of EP and EP/FRs (a, b).

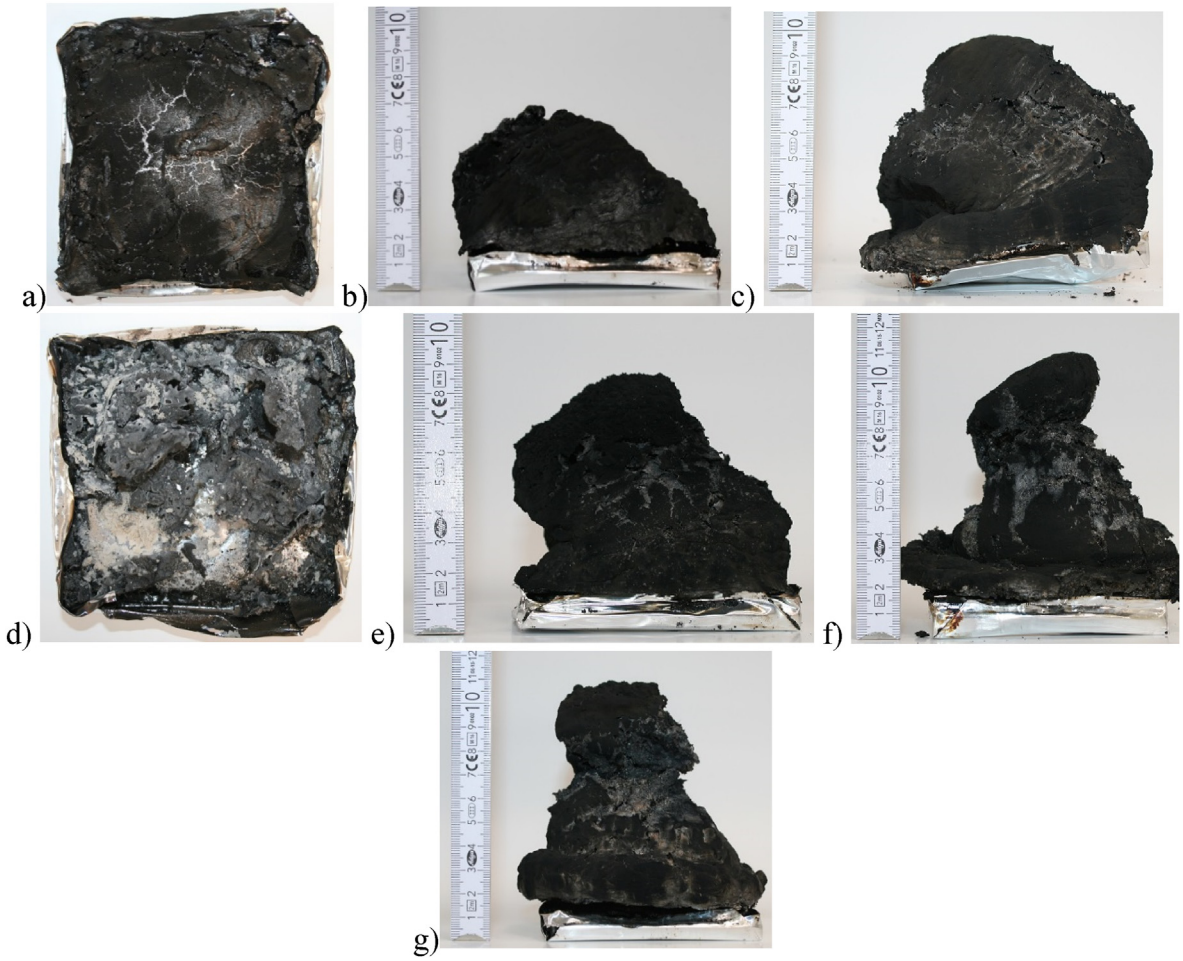

Fig. 10. Photographs of EP (a), 20APP (b), 20LHP (c), 20HS (d), 15HS/15LHP (e), 10HS/10LHP (f), 5HS/15LHP (g) after cone calorimetry tests.

of incomplete combustion products. The obtained results confirm the occurrence of a synergistic effect between the hazelnut shell and L-histidinium dihydrogen phosphate-phosphoric acid.

3.5.3. Characterization of decomposition products

The TGA/FT-IR analysis provided an insight into the mechanism of the thermal decomposition of EP, EP with APP and 5SH/15LHP, conducted in air to better reflect real conditions. The 3D FT-IR results of the entire thermal decomposition process and the FT-IR spectra at Tmax are listed in Fig. 13. The absorption band presented in the 3D spectrum indicates that the gas emission started at 350 °C for the unmodified EP, at 328 °C for 20APP, and at 336 °C for 5HS/15LHP. The major gas products of the unmodified EP were water and phenol derivatives at 3650 cm-1; aromatic compounds

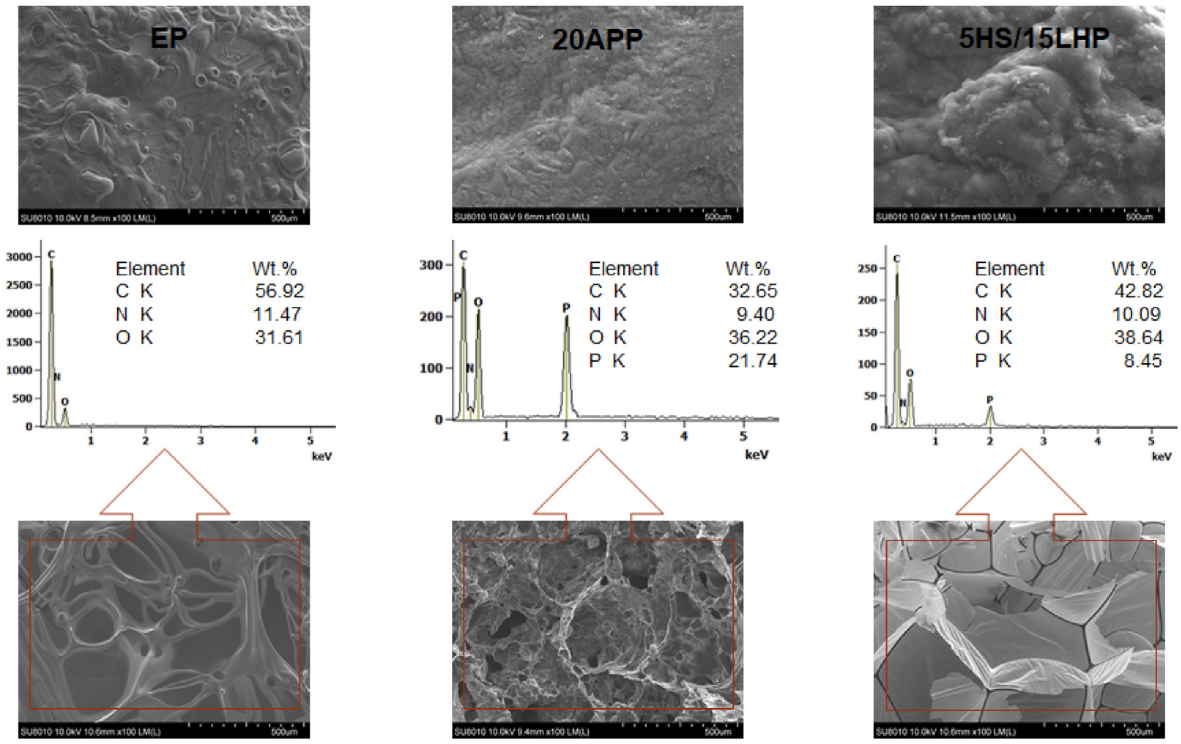

Fig. 11. SEM images of cone calorymetry residues (outer and inner), mag. 500x

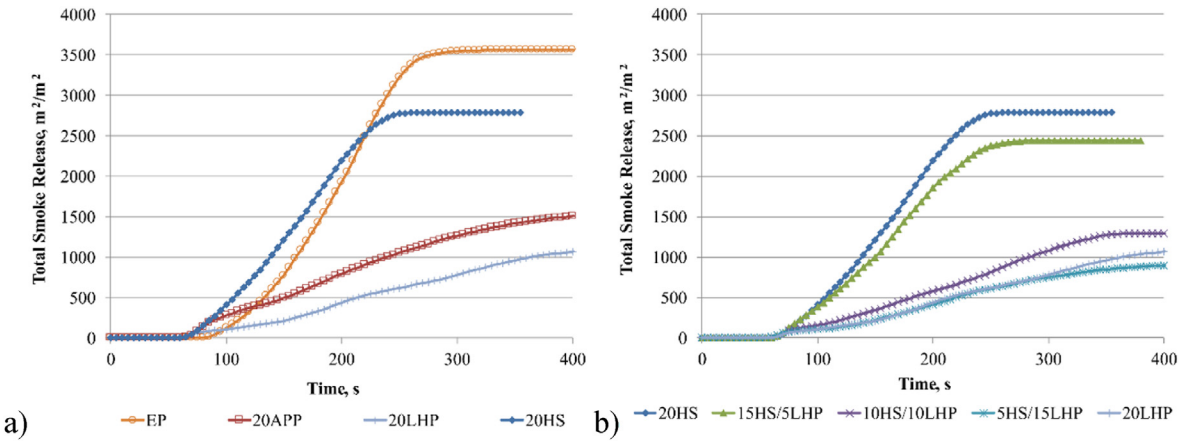

Fig. 12. Representative total smoke release curves of EP and EP/FRs (a, b).

at 3032 cm-1, 1608 cm-1, 1508 cm-1 and 1328 cm-1; hydrocarbons at 2958-2933 cm-1 and 2872 cm-1; CO_2 at 2359 cm-1 and 2322 cm-1 as well as ester or ether components at 1756 cm-1, 1259 cm-1 and 1175 cm-1 [27]. At the second gas emission at 566 °C the emission of CO_2 and CO was observed. The addition of IFRs caused the occurrence of three gas emission steps; in the first one, only low-intensity peaks corresponding to those visible on the spectra of the unmodified EP were observed. It can be concluded that the rest of the element C and aromatic compounds remain in the condensed phase and participate in the formation of char [28]. At the temperature of 328 °C the 20APP, in contrast to EP, released little to none carbonyl compounds and alkylated amines, while the release of other major products such as phenol and BPA was reduced [29]. Signals at 965 cm-1 and 930 cm-1 deriving from NH3 for 20APP and 5HS/15LHP were observed, however, in the case of 5HS/15LHP the signals show very low absorbance. For 5HS/15LHP peaks connected with N-O bond and C=N group at wavenumber range 1640–1670 cm-1 [7] as well at 1260 cm-1 connected with the C-N stretching bond [30] can also be seen. Moreover, above 530 °C the peaks associated with CO2 have a higher intensity, and new peaks associated with the secretion of CO appear. In the case of 5HS/15LHP the highest absorbance of peak associated with CO_2 evolution was observed. This phenomenon led to the dilution of smoke in the burning zone.

3.5.4. Analysis of gaseous burning products

The Purser furnace was developed to study smoke and toxic combustion products evolution from polymers under different stages and types of fire [31]. Steady-state burning was achieved by delivering a sample into the furnace of increasing heat flux at a

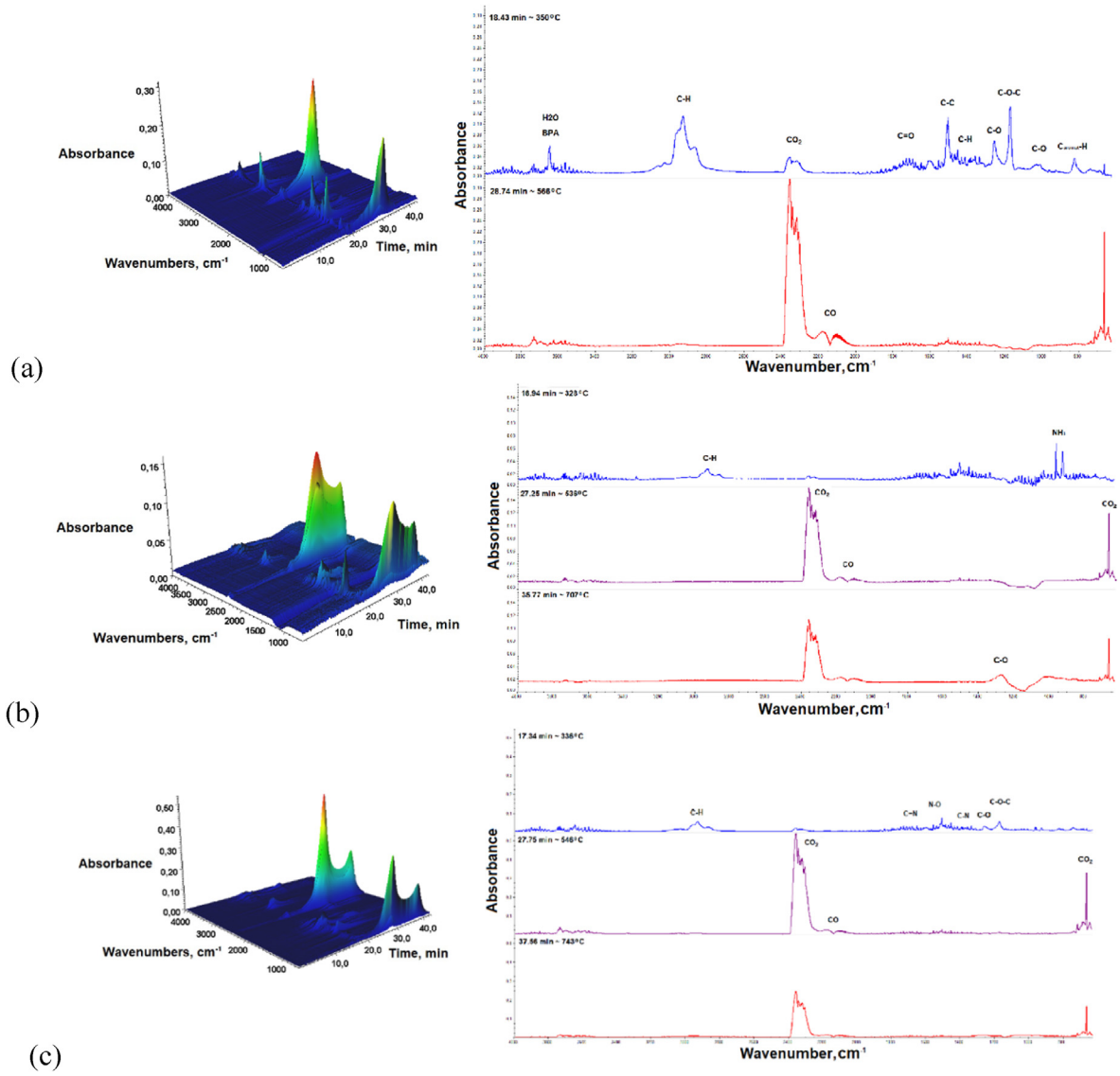

Fig. 13. The 3D infrared spectra and the FT-IR spectra at Tmax of EP (a), 20APP (b) and 5HS/15LHP (c).

fixed rate and recording the product yields over a steady-state period of the run [32]. For 5HS/15LHP three stages of gas emissions were observed (Fig. 14). In the first one, conducted at 17.32 min, the same signals were observed as in the case of the TGA/FT-IR method, but they were more intense, which is related to the conditions of the tested method. In the remaining two stages, i.e. at 25.52 and 31.88 min, the CO_2 and CO gases were detected.

3.6. Fire retardant mechanism

Based on our results and the literature it was established that the decomposition mechanism proceeds according to the diagram shown in Fig. 15. In mechanism I it was shown that the amine group detaches from the amino acid particle forming gaseous ammonium and nitrogen oxides. It is probable, that some amount of hydrogen cyanide was formed, yet it was not detected during our tests [33,34]. The acidic group typically decomposes enhancing char formation and it releases carbon oxides, water (providing the heat sink effect) and other nonflammable gases. Phosphoric acid dehydrates forming either phosphorus pentoxide or polyphosphoric acid (in lower temperatures) taking part in the char formation [22]. However, the latter is more effective than P2O5 due to its prolonged linear structure. In mechanism II according to the literature reports histidine may also undergo the inner cyclization process forming a structure consisting of two rings: 2-amino-2,4-cyclopentadien-1-one and imidazole co-creating a char structure. Production of a high amount of nonflammable gaseous products combined with a thick and strong char structure isolates the sample from the heat. This results in a lesser amount of flammable hydrocarbons in the combustion zone and lower calorimetric parameters. On the other hand, the presence of HS increases the char yield and affects its highly swollen structure with numerous closed cells, which prevent the release of decomposition products into the combustion zone. The char formed after burning the resin modified with HS creates a three-dimensional, leaky structure (Fig. S5 b). The resin with LHP creates a porous structure with numerous collapsed pores (Fig. S5 a). Their combination creates a thin-walled structure embed on a skeleton formed by HS (Fig. 11). The optimal composition of the developed fire retardant system is a 1:3 ratio that allows for obtaining the most desirable structure (Fig. S5 c and d).

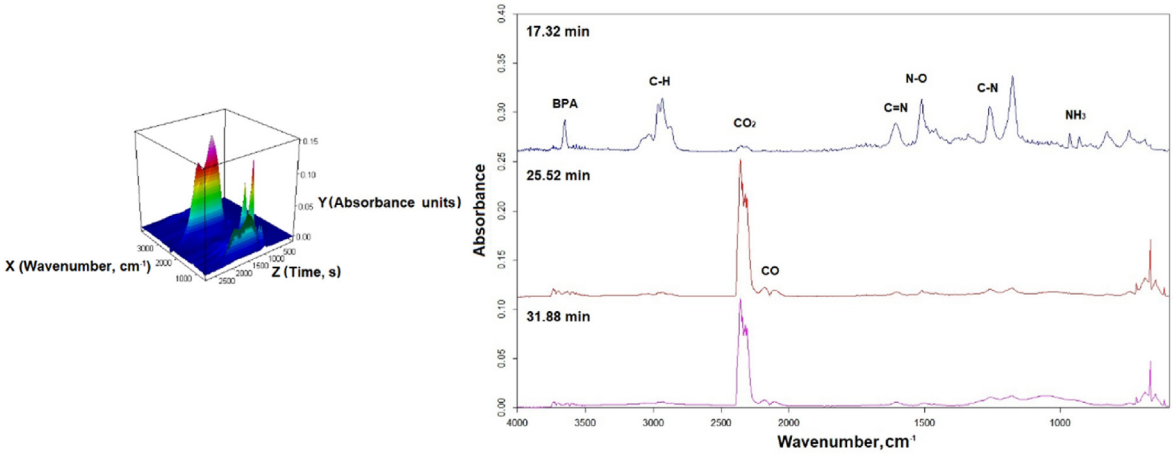

Fig. 14. 3D infrared spectrum for the emitted gases for 5HS/15LHP.

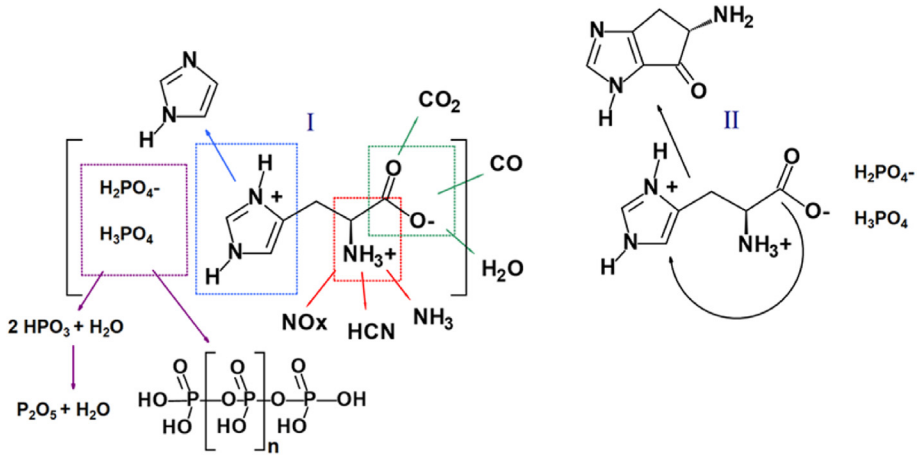

Fig. 15. Proposed decomposition mechanism for LHP.

4. Conclusions

In the study a new intumescent fire retardant system based on a hazelnut shell and L-histidinium dihydrogen phosphate-phosphoric acid was introduced to epoxy resin and examined. It was found that the mixing process, conducted using a high-speed mechanical stirrer, allowed for the occurrence of a synergistic effect between HS and LHP. The EP modified with the developed fire retardant system was characterized by greater thermal stability, which was confirmed by the delay in the onset temperature of decomposition, lower decomposition rate and the formation of a significant yield of residue. The lowest flammability and smoke emission were noted for the material containing 5 wt% of ground hazelnut shell and 15 wt% of L-histidinium dihydrogen phosphate-phosphoric acid. That mixture ratio supported the formation of a large swollen structure with numerous closed cells inside the char. Moreover, the developed fire retardant system reduced the emission of toxic decomposition products, mainly NH3 and CO in favor of CO_2, compared to the reference materials.

CRediT authorship contribution statement

K. Salasinska: Conceptualization, Investigation, Methodology, Formal analysis, Visualization, Resources, Writing - original draft, Writing - review & editing, Project administration, Funding acquisition. **M. Celiński:** Conceptualization, Funding acquisition, Resources, Software, Writing - original draft, Writing - review & editing. **K. Mizera:** Formal analysis, Investigation, Writing - original draft, Writing - review & editing, Writing - original draft. **P. Kozikowski:** Investigation, Funding acquisition. **M.K. Leszczyński:** Investigation, Writing - original draft. **A. Gajek:** Supervision.

Declaration of competing interest

The authors declare that they have no known competing financial interests or personal relationships that could have appeared to influence the work reported in this paper.

Acknowledgement

Publication on the results of the research task I-56 was conducted under the statutory activities of CIOP – PIB, and also realized with equipment allocated in WUT and IPC PAS.

Appendix A. Supplementary data

Supplementary data to this article can be found online at https://doi.org/10.1016/j.polymdegradstab.2020.109292.

References

[1] Y.J. Xu, L. Chen, W.H. Rao, M. Qi, D.M. Guo, W. Liao, Y.Z. Wang, Latent curing epoxy system with excellent thermal stability, flame retardance and dielectric property, Chem. Eng. J. 347 (2018) 223–232.

[2] Y. Wen, Z. Chen, W. Li, Z. Li, D. Liao, X. Hu, N. Pan, D. Wang, T.R. Hull, A novel oligomer containing DOPO and ferrocene groups: synthesis, characterization, and its application in fire retardant epoxy resin, Polym. Degrad. Stabil. 156 (2018) 111–124.

[3] X. Zhang, Q. He, H. Gu, H.A. Colorado, S. Wei, Z. Guo, Flame-retardant electrical conductive nanopolymers based on bisphenol F epoxy resin reinforced with nano polyanilines, ACS Appl. Mater. Interfaces 5 (2013) 898–910.

[4] M.J. Chen, Y.C. Lin, X.N. Wang, L. Zhong, Q.L. Li, Z.G. Liu, Influence of cuprous oxide on enhancing the flame retardancy and smoke suppression of epoxy resins containing microencapsulated ammonium polyphosphate, Ind. Eng. Chem. Res. 54 (2015) 12705–12713.

[5] J. Wan, B. Gan, C. Li, J. Molina-Aldareguia, E.N. Kalali, X. Wang, D.Y. Wang, A sustainable, eugenol-derived epoxy resin with high biobased content, modulus, hardness and low flammability: synthesis, curing kinetics and structure–property relationship, Chem. Eng. J. 284 (2016) 1080–1093.

[6] Y. Wang, S. Zhang, X. Wu, Ch Lu, Y. Cai, L. Ma, G. Shi, L. Yang, Effect of montmorillonite on the flame-resistant and mechanical properties of intumescent flame-retardant poly(butylene succinate) composites, J. Therm. Anal. Calorim. 128 (2017) 1417–1427.

[7] R.K. Jian, Y.F. Ai, L. Xia, Z.P. Zhang, D.Y. Wang, Organophosphorus heteroaromatic compound towards mechanically reinforced and low-flammability epoxy resin, Comp. Part B 168 (2019) 458–466.

[8] X. Mu, J. Zhan, Ch Ma, Y. Pan, F. Chu, L. Song, Y. Hu, Integrated effect of flame retardant wrapped macromolecular covalent organic nanosheet on reduction of fire hazards of epoxy resin, Comp. Part A 117 (2019) 23–33.

[9] J.C. Markwart, A. Batting, M.M. Velencoso, D. Pollok, B. Schartel, F.R. Wurm, Aromatic vs. aliphatic hyperbranched polyphosphoesters as flame retardants in epoxy resins, Molecules 24 (2019) 3901.

[10] K. Sałasińska, A. Gajek, M. Celiński, K. Mizera, M. Borucka, K. Duszak, Thermal stability of epoxy resin modified with developed flame retardant system based on renewable raw materials, Mater. Sci. Forum 995 (2020) 43–48.

[11] K. Sałasińska, M. Barczewski, M. Borucka, R.L. Górny, P. Kozikowski, M. Celiński, A. Gajek, Thermal stability, fire and smoke behaviour of epoxy composites modified with plant waste fillers, Polymers 11 (2019) 1234.

[12] Patent Application P.426677K.

[13] K. Sałasińska, Kompozyty Polimerowe Z Napełniaczami Pochodzenia Roślinnego Otrzymywane Z Materiałów Odpadowych, PhD Thesis Warsaw University of Technology, 2015.

[14] K. Sałasińska, M. Celiński, P. Kozikowski, M.K. Leszczyński, M. Borucka, A. Gajek, Influence of the developed flame retardant system based on renewable raw materials on epoxy resin fire behavior, Mater. Sci. Forum 995 (2020) 37–42.

[15] I. Mata, E. Espinosa, E. Molins, S. Veintemillas, S. Maniukiewicz, C. Lecomte, A. Cousson, W. Paulus, Contributions to the application of the transferability principle and the multipolar modeling of H atoms: electron-density study of L-histidinium dihydrogen orthophosphate orthophosphoric acid, Acta Crystallogr. A 62 (2006) 365–378.

[16] X. Wang, Y. Hu, L. Song, H. Yang, B. Yu, B. Kandola, D. Deli, Comparative study on the synergistic effect of POSS and graphene with melamine phosphate on the flame retardance of poly(butylene succinate), Thermochim. Acta 543 (2012) 156–164.

[17] K. Sałasińska, M. Celiński, M. Barczewski, M.K. Leszczyński, M. Borucka, P. Kozikowski, Fire behavior of flame retarded unsaturated polyester resin with high nitrogen content additives, Polym. Test. 84 (2020), 106379.

[18] K. Sałasińska, M. Barczewski, R. Górny, A. Kloziński, Evaluation of highly filled epoxy composites modified with walnut waste filler, Polym. Bull. 75 (2018) 2511–2528.

[19] X. Ma, W. Guo, Z. Xu, S. Chen, J. Cheng, J. Zhang, M. Miao, D. Zhang, Synthesis of degradable hyperbranched epoxy resins with high tensile, elongation, modulus, and low-temperature resistance, Comp. Part B 192 (2020), 108005.

[20] M.R. Ricciardi, I. Papa, A. Langella, T. Langella, V. Lopresto, V. Antonucci, Mechanical properties of glass fibre composites based on nitrile rubber toughened modified epoxy resin, Comp. Part B 139 (2018) 259–267.

[21] K. Sałasińska, K. Mizera, M. Celiński, P. Kozikowski, M. Borucka, A. Gajek, Thermal properties and fire behavior of a polyethylene with mixture of copper phosphate and melamine phosphate as novel flame retardant, Fire Saf. J. 115 (2020), 103137.

[22] J. Naveen, M. Jawaid, E.S. Zainudin, M.T.H. Sultan, R. Yahaya, M.S.A. Majid, Thermal degradation and viscoelastic properties of Kevlar/Cocos nucifera sheath reinforced epoxy hybrid composites, Compos. Struct. 219 (2019) 194–202.

[23] J.C. Markwart, A. Battig, L. Zimmermann, M. Wagner, J. Fischer, B. Schartel, F.R. Wurm, Systematically controlled decomposition mechanism in phosphorus flame retardants by precise molecular architecture: P–O vs P–N, ACS Appl. Polym. Mater. 1 (2019) 1118–1128.

[24] A. Ramgobin, G. Fontaine, C. Penverne, S. Bourbigot, Thermal stability and fire properties of salen and metallosalens as fire retardants in thermoplastic polyurethane (TPU), Materials 10 (2017) 665.

[25] S. Huo, Z. Liu, Ch Li, X. Wang, H. Cai, J. Wang, Synthesis of a phosphenanthrene/benzimidazole-based curing agent and its application in flame-retardant epoxy resin, Polym. Degrad. Stabil. 163 (2019) 100–109.

[26] M. Kurańska, A. Prociak, S. Michałowski, K. Zawadzińska, The influence of blowing agents type on foaming process and properties of rigid polyurethane foams, Polimery-W 63 (2018) 672–678.

[27] L. Liu, Y. Xu, M. Xu, Z. Li, Y. Hu, B. Li, Economical and facile synthesis of a highly efficient flame retardant for simultaneous improvement of fire retardancy, smoke suppression and moisture resistance of epoxy resins, Compos. Part B. 167 (2019) 422–433.

[28] K. Salasinska, K. Mizera, M. Barczewski, M. Borucka, M. Gloc, M. Celiński, A. Gajek, The influence of degree of fragmentation of *Pinus sibirica* on flammability, thermal and thermomechanical behavior of the epoxy-composites, Polym. Test. 79 (2019), 106036.

[29] P. Muller, M. Morys, A. Sut, Ch Jager, B. Illerhaus, B. Schartel, Melamine poly(zinc phosphate) as flame retardant in epoxy resin: decomposition pathways, molecular mechanisms and morphology of fire residues, Polym. Degrad. Stabil. 130 (2016) 307–319.

[30] A.D. Naik, G. Fontaine, F. Samyn, X. Delva, J. Louisy, S. Bellayer, Y. Bourgeois, S. Bourbigot, Outlining the mechanism of flame retardancy in polyamide 66 blended with melamine-poly(zinc phosphate), Fire Saf. J. 70 (2014) 46–60.

[31] M. Sankowska, A. Gajek, M. Celiński, K. Sałasińska, Determination of gaseous products of thermal degradation of thiram, J. Therm. Anal. Calorim. 128 (2017) 1639–1647.

[32] A.A. Stec, T.R. Hull, K. Lebek, Characterization of the steady state tube furnace (ISO TS 19700) for fire toxicity assessment, Polym. Degrad. Stabil. 93 (2008) 2058–2065.

[33] A. Schaberg, R. Wroblowski, R. Goertz, Comparative study of the thermal decomposition behaviour of different amino acids and peptides, J. Phys.: Conf. Ser. 1107 (2018), 032013.

[34] I.M. Weiss, C. Muth, R. Drumm, Thermal decomposition of the amino acids glycine, cysteine, aspartic acid, asparagine, glutamic acid, glutamine, arginine and histidine, BMC Biophys. 11 (2018) 2.